Computing von Kries Illuminant Changes by Piecewise Inversion of Cumulative Color Histograms

Michela Lecca* and Stefano Messelodi*

* *Fondazione Bruno Kessler, Center for Scientific and Technological Research, via Sommarive 18, Povo, 38100 Trento, Italy*

Abstract

We present a linear algorithm for the computation of the illuminant change occurring between two color pictures of a scene. We model the light variations with the von Kries diagonal transform and we estimate it by minimizing a dissimilarity measure between the piecewise inversions of the cumulative color histograms of the considered images. We also propose a method for illuminant invariant image recognition based on our von Kries transform estimate.

Key Words: Color Image Analysis, Color Histograms, Illuminant Changes, von Kries Model, Image Retrieval.

1 Color across Light

The color of an image recorded by a camera depends on the spectral power of the light illuminating the scene, on the geometrical and physical conditions of the scene and on the characteristics of the device used for the acquisition. Therefore, the same scene viewed under two different illuminants produces two different color images. For instance, a white object appears white in the daily light, but red when illuminated by a red light. In the human vision system, the illuminant invariance is achieved by the *color constancy* process. This is a chromatic adaptation mechanism, that detects and removes possible chromatic dominants and illuminant incidents from the observed scene, so that the same scene under different illuminants is perceived as the same entity [20].

Color is one of the most widely used features in many computer vision fields, like image retrieval and indexing [27], image segmentation [25] and object tracking [10], but its instability with respect to changes of light adversely affects the performances of the algorithms based on its analysis. To overcome this problem, many methods for discounting the illuminant color sensitivity from an image have been developed. For instance, the color enhancement algorithms, as the well known Gray-World algorithm, the comprehensive color normalization [16], the Retinex theory [22], [14], and the automatic color enhancement (ACE) [8], discard the color illuminant dependency by processing the image in the color space and transforming its color. In other methods, like the gamut mapping approaches [3], the color-by-correlation techniques [5], and the machine learning strategies as [6], [9], [1], the color constancy is achieved by computing the transformation relating the illuminant of the input image and a reference canonical illuminant. The input image is therefore remapped as it was taken under the known canonical illuminant. Color constancy can be obtained also without modifying or

remapping on to a standard reference the input image, but simply by describing it by a set of illuminant invariant features, like the color invariant histograms proposed in [7], [15] and [17] or the edge-based features employed in [23] and [19]. However, the algorithmic simulation of the human color constancy mechanism is a hard problem: generally, the algorithms make strong assumptions circumscribing their usage, like hypotheses about the uniformity of the illuminant, the characteristics of the device used for recording the scene, the number and the position of the light sources, the reflectance properties of the materials in the scene. Moreover, many methods, as for instance ACE, use thresholds to be fixed empirically, while the machine learning techniques need for the choice of a training set and of a training phase, that is often computationally expensive. A comparison of the most used computational color constancy algorithms is presented in [29] and [31].

In this work, we propose a novel algorithm for estimating the illuminant change occurring between an image of a scene and a re-lighted version of it, so that color constancy is achieved by remapping the re-lighted image on its canonical reference. We assume that the illuminant variation is homogeneous over the whole image and we approximate it by the von Kries transform [18]. These hypotheses are assumed by a lot of color constancy algorithms. We represent the colors of each image by the histograms of the three channels red, green, blue, and we define a *piecewise inversion* of the cumulative channels histograms. We compute the von Kries light variation by minimizing a measure of dissimilarity between the piecewise inversions of the cumulative color histograms of the images considered. The color representation by histograms makes the method robust to image rescaling and in-plane rotating. Our approach is very efficient from the computational point of view, also in comparison with other techniques discussed in the Sections 4.4 and 4.5: no user interaction is requested, except for setting up two integer numbers N and M regarding the color quantization and the algorithm complexity is linear with respect to the number of image pixels and to the sum $N + M$. Moreover, differently from many color constancy algorithms requiring the usage of a particular color space like [5], [3], [4], our algorithm works directly in the RGB color space.

We also illustrate how our estimate can be used for the illuminant invariant image recognition. The problem is stated as follows: given a set of known images, said *references*, and an unseen image, termed *query*, we want to find the reference that, if re-lighted, is the most similar to the query. To solve this problem, we firstly compute the von Kries transform possibly relating the query and each reference, and then we select the reference I whose relighted version is the most similar to the query. The similarity we use here is defined in the space of the piecewise inversion of the cumulative color histograms of the query and of the references.

The tests carried out on synthetic and real-world datasets showed good performances both for our illuminant estimate and for its application to image recognition. The paper is organized as follows: Section 2 illustrates the von Kries diagonal model, Section 3 explains our technique for estimating the illuminant changes; Section 4 describes the experiments measuring the accuracy on the von Kries transform estimate; Section 5 presents an illuminant invariant image recognition strategy based on our estimate of illuminant variations; finally Section 6 outlines our conclusions and future work.

2   The von Kries Diagonal Model

The response of a camera to the light reflected from a point in a scene is coded in a triplet (p_0, p_1, p_2), with for each $i = 0, 1, 2$

$$p_i = \int_\Omega E(\lambda) S(\lambda) F_i(\lambda) \, d\lambda. \tag{1}$$

In this formula, λ is the wavelength of the light illuminating the scene, E its spectral power distribution, S the bidirectional reflectance distribution function (BRDF) of the illuminated surface to which the point belongs, and F_i is the spectral sensitivity function of the sensor. The integral ranges over the visible spectrum, i.e. $\Omega = [380, 780]$ nm.

The BRDF depends on the directions on the incoming and of the reflected light. For a wide range of matte surfaces, which appear equally bright from all viewing directions, the BRDF is well approximated by the

Lambertian photometric reflection model [12]. Moreover, as proved in [24], under this assumption, the surface reflectance can be expressed by a linear combination of three basis functions $S^k(\lambda)$ with weights σ_k, $k = 0, 1, 2$, so that equation (1) can be re-written as follows:

$$\mathbf{p}^T = W\sigma^T \tag{2}$$

where $\mathbf{p} = (p_0, p_1, p_2)$, $\sigma = (\sigma_0, \sigma_1, \sigma_2)$, and W is the 3×3 matrix with entry $W_{ki} = \int_\Omega E(\lambda)S^k(\lambda)F_i(\lambda)d\lambda$, ($k$, $i = 0, 1, 2$).

The response $\mathbf{p}' = (p'_0, p'_1, p'_2)$ captured under an illuminant with spectral power E' is then given by $\mathbf{p}'^T = W'\sigma^T$. Therefore, since the spectral reflectance of the surface in the scene does not depend on the illumination, the responses $\mathbf{p}$ and $\mathbf{p}'$ are related by the linear transform

$$\mathbf{p}^T = W[W']^{-1}\mathbf{p}'^T. \tag{3}$$

Note that Equation (3) makes sense only when the matrix W' is not singular, i.e. when the functions E', S^k and F^k ($k = 0, 1, 2$) differ from the null function. Since we assume that the surface reflectance and the camera responses are not identically zero, the inverse of W' exists when $E' \neq 0$ for all wavelengths.

The von Kries diagonal model we use in this work, approximates the spectral sensitivity of the camera sensor by the delta function, i.e. it assumes that each sensor responds only to a single wavelength of light: $F_i(\lambda) = \delta(\lambda - \lambda_i)$, for each $i = 0, 1, 2$. Under this assumption, Equation (3) becomes

$$(p_0, p_1, p_2) = \left(\frac{E(\lambda_0)}{E'(\lambda_0)}p'_0, \frac{E(\lambda_1)}{E'(\lambda_1)}p'_1, \frac{E(\lambda_2)}{E'(\lambda_2)}p'_2 \right) \tag{4}$$

i.e. the von Kries diagonal model approximates the change of illuminant mapping $\mathbf{p}$ onto $\mathbf{p}'$ by a simple linear transformation that rescales each channel independently.

In the following, for each $i = 0, 1, 2$, we set $\alpha_i := E(\lambda_i)[E'(\lambda_i)]^{-1}$ and we refer to the parameters α_0, α_1 and α_2 as the *von Kries coefficients*.

The diagonal model has been proved to be a good approximation for the illuminant changes [18], especially in the case of narrow-band sensory systems, and it is assumed by many color constancy algorithms, like the Gray-World and the gamut mapping based approaches.

3   Computing von Kries Transform

In our method, the color of an image is described by the triplet $\mathbf{H} := (H_0, H_1, H_2)$ of the distributions of the sensory responses p_0 (red), p_1 (green), p_2 (blue). The values of p_i range on [0, 255], for $i = 0, 1, 2$. We refer to $\mathbf{H}$ as *color distribution*, whereas we call its components *channel distributions*. We consider now a continuous treatment, that allows to handle straightforward the concepts of piecewise function inversion. Hereafter we assume that

$$\int_0^{255} H_i(x) \, dx = 1, \qquad \forall \; i = 0, 1, 2. \tag{5}$$

Let H be a channel distribution. We define the cumulative channel distribution of H as the function

$$\Phi : [0, 255] \rightarrow [0, 1] \quad \text{such that} \quad \Phi(x) = \int_0^x H(y), \tag{6}$$

where x ranges over [0, 255]. Function Φ is monotonically increasing, continuous and generally not injective. In fact if H is zero on an interval $J \subset [0, 255]$, then the *restriction* * of Φ on J is constant and equal to $\Phi(\min(J))$. In this case, there exists a partition $t_0 < t_1 < t_2 < \ldots < t_n$ of [0, 255] with $t_0 = 0$, $t_n = 255$, such

---

*The restriction of a function $f \colon X \to Y$ to a subset S of X is the function $f_{|S}$ from S to Y such that $f_{|S}(s) = f(s)$ for all s in S.

that Φ is strictly monotonically increasing (resp. constant) on the ith interval and constant (resp. strictly monotonically increasing) on the $(i+1)$th interval and $i = 0, \ldots, n-1$. We note that $[0, 1] = \cup_{j=0,\ldots,n-1} \Phi([t_j, t_{j+1}))$, i.e. the set $\{\Phi([t_j, t_{j+1})\}_{j=0,\ldots,n-1}$ is a partition of $[0, 1]$.

Without loss of generality, we can suppose that Φ is strictly monotonically increasing on the ith interval and constant on the $(i + 1)$th interval. We define the following function:

$$\Psi : [0, 1] \rightarrow [0, 255] \tag{7}$$

such that the restriction of Ψ to each interval $\Phi([t_j, t_{j+1}))$ is the restriction of Φ^{-1} on $[\Phi(t_j), \Phi(t_{j+1}))$, i.e. for each j,

$$\Psi(y) = \Phi^{-1}(y), \qquad \forall\ y \in \Phi([t_j, t_{j+1})). \tag{8}$$

Function Ψ is the *piecewise* inversion of the cumulative channel distribution H. It is piecewise continuous and since it is the inverse of a monotonically increasing function, it is monotonically increasing on each interval $[\Phi(t_j), \Phi(t_{j+1}))$. This implies that it is integrable too.

If Φ is bijective, we simply consider the trivial partition $[t_0, t_1] = [0, 255]$ and we take $\Psi = \Phi^{-1}$. Let H and H' be the distributions of a channel of two images I and I' respectively. If the two images represent the same scene under two different illuminant, i.e. if there exists α in $(0, +\infty)$ such that $H(\frac{1}{\alpha}x) = H'(x)$ for each x in $[0, 255]$, we have that $\Phi'(x) = \Phi(\alpha x)$ and $\Psi'(y) = \frac{1}{\alpha}\Psi(y)$, for all $y \in [0, 1]$. We estimate the von Kries coefficient α by minimizing the L^2 distance between the functions Ψ and $\alpha\Psi'$:

$$\delta = \int_0^1 (\Psi(y) - \alpha\Psi'(y))^2\ dy. \tag{9}$$

In our implementation, the channel distributions are represented by histograms of N bins, where N ranges in $\{1, \ldots, 256\}$. Thus Equation (3) becomes $\sum_{x=1}^N H_i(x) = 1$, for each $i = 0, 1, 2$. The piecewise inversions of the cumulative distributions are quantized on a grid of M nodes equi-spaced on the interval $[0, 1]$, so that formula (9) becomes

$$\delta = \sum_{y=1}^{M-1} \left[\Psi\left(\frac{y}{M}\right) - \alpha\Psi'\left(\frac{y}{M}\right)\right]^2. \tag{10}$$

The von Kries coefficient α is hence given by

$$\alpha = \frac{\sum_{y=1}^{M-1} \Psi'\left(\frac{y}{M}\right)^2}{\sum_{y=1}^{M-1} \Psi\left(\frac{y}{M}\right)\Psi'\left(\frac{y}{M}\right)}. \tag{11}$$

Note that the Mth bin is excluded from the computation of δ. In fact, since the values of p_0, p_1, p_2 range in $[0, 255]$, the values of $\alpha_0 R_0$, $\alpha_1 G_0$, $\alpha_2 B_0$ that are greater than 255 are cast to 255 (*saturated pixels*). Therefore, to make the estimate of the von Kries coefficients robust (as much as possible) with respect to the pixel saturation, the Mth value of the functions Ψ and Ψ' are not considered. However, it is clear that the performances decrease by incrementing the number of saturated pixels (see the experiments).

The algorithm for estimating the von Kries coefficients takes as input two images I and I' and the parameters N and M for the color quantization. It consists of three steps: (*i*) firstly it computes the color histograms of I and I', then (*ii*) the cumulative histograms and their piecewise inversions, and finally (*iii*) estimates by the equation (11) the von Kries coefficients. The algorithmic complexity of all the steps is linear. More precisely, for step (*i*), the complexity is $O(N_I + N_{I'})$, where N_I and N_I' are the number of pixels of the images I and I' respectively; for step (*ii*) it is $O(N + M)$, and for step (*iii*) it is $O(M)$. The total complexity of the proposed approach is therefore linear with respect to the numbers of image pixels and to the quantization parameters N and M.

4   Performance Evaluation

The accuracy on the estimate of the von Kries diagonal transform has been tested on different synthetic and real-world databases. In 4.1, 4.2, 4.3 we report the results obtained on the synthetic database TESTS51 [26] and on the real-world datasets ALOI [21] and BARNARD [28]. In the Subsections 4.4 and 4.5, we present a comparative analysis of our approach with other methods (BEST-FIT, the color transfer technique [4] and the color constancy methods in [31]).

Each database consists of a set of images taken under a reference illuminant (*reference images*) and a set of re-lighted versions of them (*test images*). For all the three databases, we measure the accuracy on the estimate of the von Kries transform K relating each test image I to the correspondent reference image I_0 as follows:

$$\mathcal{A} = 1 - L^1(I, K^{est}(I_0)), \tag{12}$$

where $L^1(I, K^{est}(I_0))$ is the L^1 distance computed on the RGB space between I and the transform $K^{est}(I_0)$ of I_0, and K^{est} indicates the von Kries transform we estimate. This distance has been normalized to range in [0,1]. Therefore, the closer to 1 $\mathcal{A}$ is, the better the estimate of the von Kries transform is. To quantify the benefit of our estimate, we compared the accuracy (12) with the value

$$\mathcal{A}_0 = 1 - L^1(I, I_0), \tag{13}$$

that measures the similarity of the reference to the test image when no color enhancement is applied.

The test images of TESTS51 have been generated synthetically by rescaling the RGB channels of 51 natural pictures by a set of 11 real numbers $\{\beta_w\}$ ranging in [0.5, 3.0] (see Subsection 4.1). Therefore, in addition to the values of (12) and (13), for TESTS51 we measure the precision on the estimate of the von Kries coefficients by computing the error

$$\varepsilon_w = 1 - \frac{\beta_w^{est}}{\beta_w} \qquad \forall \; w = 0, \dots, 10, \tag{14}$$

where β_w^{est} is our estimate of β_w. The closer ε_w to zero is, the better the accuracy on the determination of the von Kries transform is. A strictly negative (positive, resp.) value of ε_w indicates that the estimate is greater (smaller, resp.) than the real coefficient.

For the comparison in Subsection 4.4 we used the mean accuracies (12), while for the comparison in Subsection 4.5, we use two error measures defined in [31] and detailed next.

We measured the sensitivity of our estimates with respect to the color quantization by the mean values of (12) and (14) (averaged on the number of test images) by varying the values of N and M. More precisely, we considered $N = 256, 128, 64, 32, 16$ bins and $M = 10, 30, 50, 100$ bins. We observed that the accuracy (12) and the error (14) critically depend on N, while changing M does not affect significantly the estimation performances. Therefore, here we discuss the robustness of our method with respect to both the parameters N and M only for the synthetic dataset TESTS51, while in the experiments on ALOI and BARNARD we fixed $M = 100$ and we vary N.

4.1   TESTS51

The dataset TESTS51 is freely available at `http://www-cvr.ai.uiuc.edu/ponce_grp/data/`. It consists of a set of images of 8 different objects and of a set of 51 test-pictures in which the objects appear under different conditions (occluded, rescaled, rotated, differently illuminated, ...).

In this work, we took the 51 test pictures as references and we generated synthetically the test images by changing the color appearance of each reference by the von Kries transforms

$$F_{\beta_w}(p_0, p_1, p_2) = \beta_w(p_0, p_1, p_2), \tag{15}$$

(a)   (b)
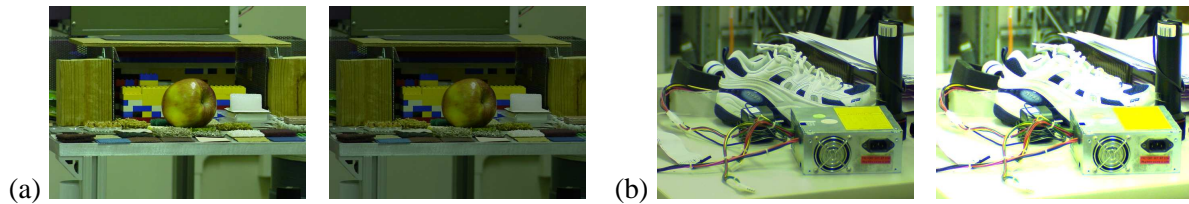
Figure 1: TESTS51 Database: the Ponce's pictures on left in (a) and (b) have been transformed by rescaling their color channels by (a) 0.6 and (b) 1.8. Their re-lighted versions are shown on right.

with $\beta_w = 0.5 + 0.25w$, and $w = 0, \ldots, 10$. Some examples are shown in Figure 1.

Figure 2 shows the mean errors (14) and the mean accuracies (12) versus the color quantization, for $N = 256, 32, 16$ and $M = 10, 30, 50, 100$. In this figure, we omit to show the results obtained for $N = 128$ and $N = 64$ because they are very similar to those obtained for $N = 256$. We note that apart from the case $M = 10$, for $N = 256$, the error is negative for $\beta_w < 1$, positive otherwise. On the contrary, for $M \neq 10$ and $N = 64, 32, 16$, the error is positive for $\beta < 1$, negative otherwise. This behavior is due to the color quantization and to the algorithm used for minimizing (9). Clearly, for $\beta_w = 1.0$, F_{β_w} is the identity function and so the accuracy is 1.0 and the error is 0.0 for every quantization.

Figure 3 shows the mean accuracy (13) and the values of (12) for different color quantizations. By increasing β_w, the number of saturated pixels increases too, and consequently the accuracy on our estimate decreases. This is more noticeable for $\beta_w \geq 1.75$, i.e. when the brightness of the test images is 1.75 times that of the correspondent references. The best results are obtained for $N = 256$, and $M = 100$: for this color quantization, the accuracy (12) between the test images and the color-remapped references are on average 10 times smaller than the value (13) between the tests and the references. No remarkable differences are obtained by using $M = 30$, $M = 50$ or $M = 100$, while for $M = 10$ the performances are not satisfactory.

4.2 ALOI

The database ALOI is a collection of 110,250 images of 1,000 objects recorded under different circumstances. It is freely available at `http://staff.science.uva.nl/~aloi/`. Each frontal object view has been taken under 12 different light conditions, produced by varying the color temperature of five lamps illuminating the scene. More precisely, the lamp voltage was controlled to be $V_j = j \times 0.047$ Volts with $j \in J = \{110, 120, 130, 140, 150, 160, 170, 180, 190, 210, 230, 250\}$. An example of an object view under the 12 different lights is shown in Figure 4.

For each pair of illuminants (V_j, V_k) with $j \neq k$, we took the images captured with lamp voltage V_j as references and those captured with voltage V_k as tests. Therefore, we considered 132 pairs of reference and test sets.

For ALOI we do not know the actual values of the von Kries coefficients that approximate the considered changes of light. Therefore, we cannot measure the accuracy of our estimates of α_i by the formula (14). For shortness, we report only the values obtained with $N = 256$ bins in the Table (4) at the end of this paper. A more detailed analysis about the result dependency on N can be found in the Technical Report [32].

Figure 5 shows for all the sets of references and tests the mean accuracy (13) and the values of (12) when $N = 256$. As reported in [32], the mean accuracies do not change remarkably when $N = 128$ or $N = 64$, and the worst results are obtained for $N = 16$.

4.3 BARNARD

In this Section we report the experiments carried out on the real-world image dataset [28] downloadable from `http://www.cs.sfu.ca/~colour/`.
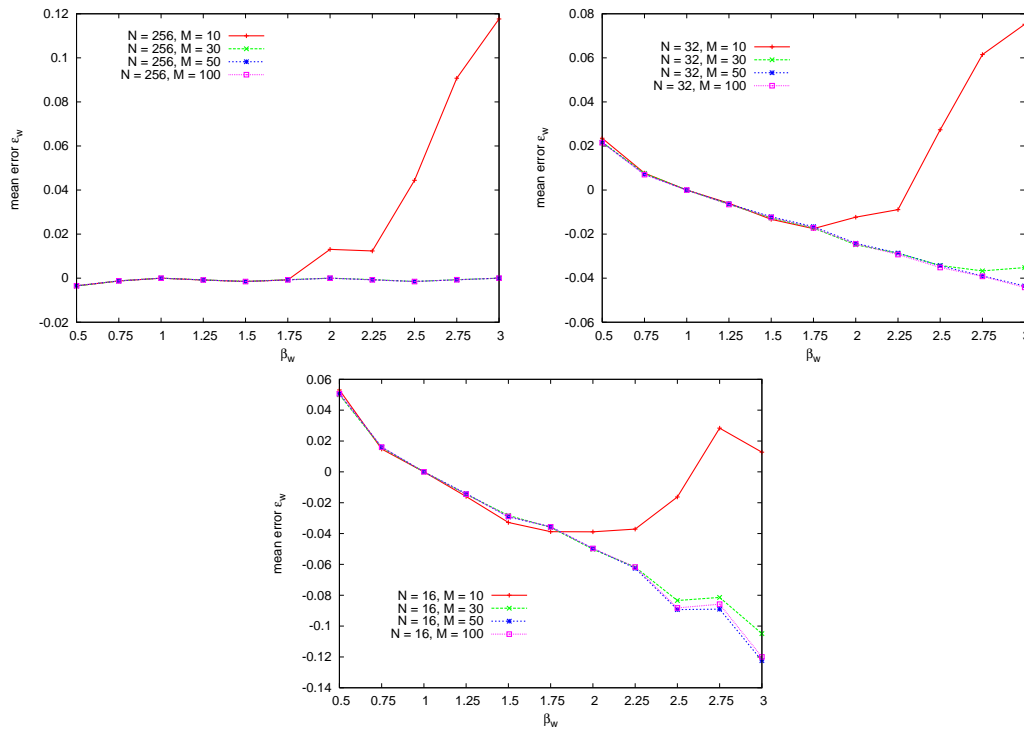
Figure 2: TESTS51: Errors (see formula (14)) on estimates of von Kries coefficients for different color quantization.
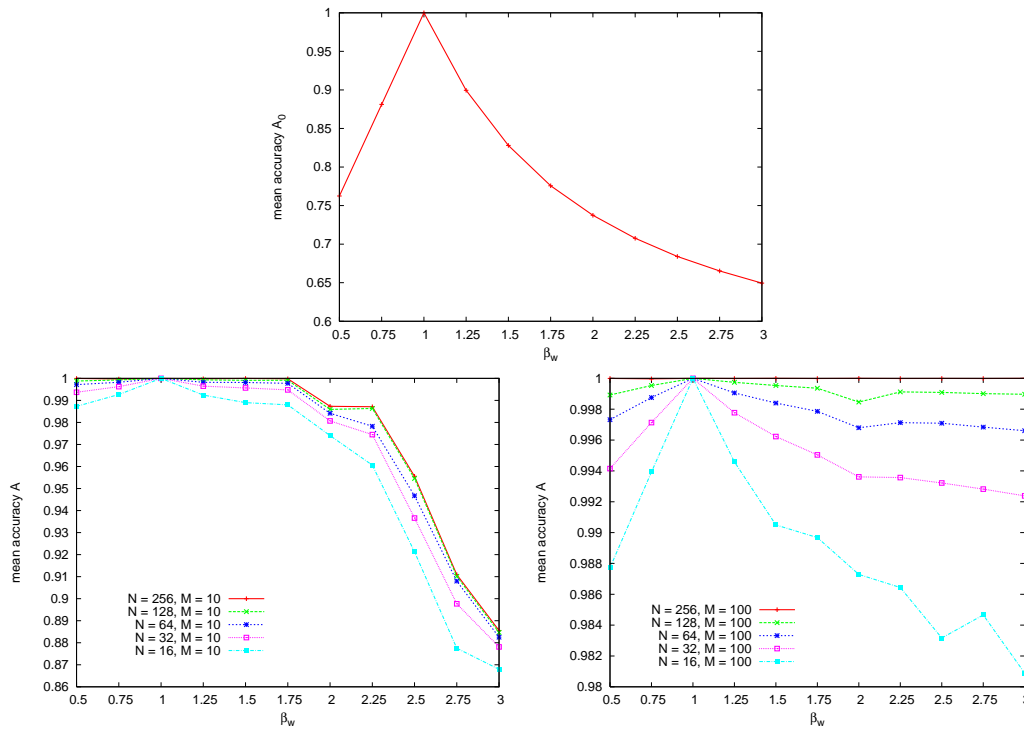

Figure 3: TESTS51: Mean Value of the accuracies (13) (top) and (12) (bottom) for different color quantizations.

Figure 4: ALOI: An example of a frontal view of an object of ALOI database taken under 12 different illuminants.
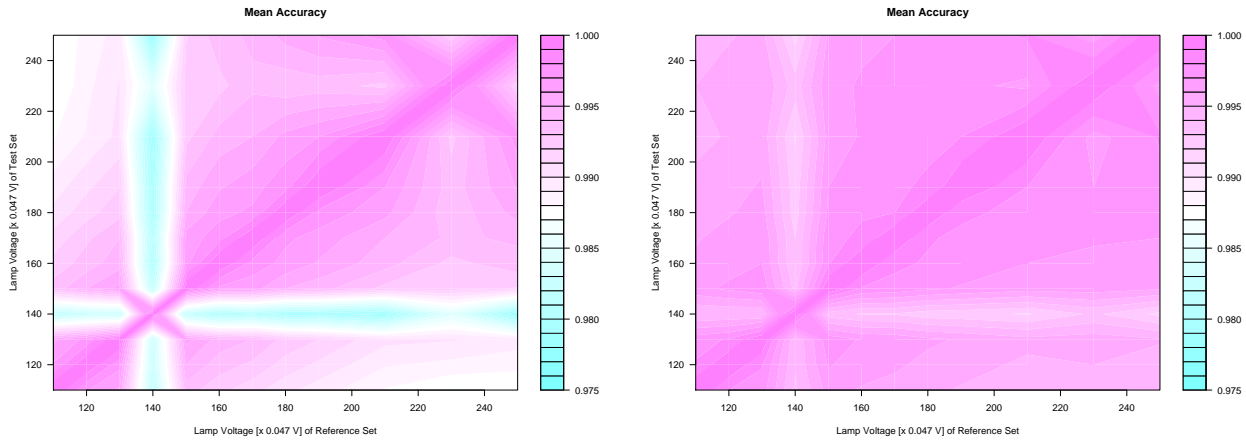

Figure 5: ALOI: Values of the mean accuracy (13) (on left) and (12) (on right). Here $N = 256$, $M = 100$. To make the plots more readable, we show a linear interpolation of the accuracy surface by colors.

This database - that we refer as BARNARD - is composed by 321 pictures grouped in 30 categories. Each category contains a reference image taken under an incandescent light Sylvania 50MR16Q (*canonical illuminant*) and a number (from 2 to 11) of relighted versions of it (test images) under different lights. The illuminant is specified image by image by a triplet (p_0, p_1, p_2).

We computed the accuracy of our estimates by the formulas (12) and (13). The results are shown in Figure 6 for different values of N, while $M = 100$, while Table 1 shows the estimated coefficients of the von Kries transform mapping the test images on to the references for $N = 256$, and $M = 100$.

4.4   Comparison with BEST-FIT and with a Color Transfer Method

When the test and the reference images are related just by an uniform change of light, and no rescaling and changes of in-plane orientation occur, the von Kries transform approximating the illuminant variation can be estimated by a *best fit* method (BEST-FIT for short), that we explain here.

Let $\mathbf{p_i}^r$ and $\mathbf{p_i}^t$ be the sensory responses at the ith pixel of the reference and test images respectively, and let $(\mathbf{p_i}^r)_j$ and $(\mathbf{p_i}^t)_j$ indicate their jth component ($j = 0, 1, 2$). By the von Kries model, $(\mathbf{p_i}^r)_j = \alpha_j(\mathbf{p_i}^t)_j$, where α_j is the jth von Kries coefficient.

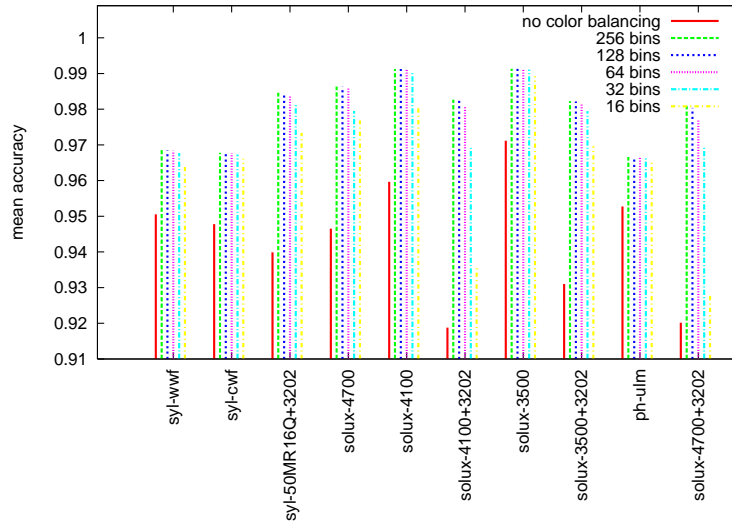For each j, BEST-FIT estimates the value of α_j by the least square method that minimizes the energy functional

$$\sum_{\mathbf{i}=1,...,N_I} [(\mathbf{p_i}^r)_j - \alpha_j(\mathbf{p_i}^t)_j]^2. \tag{16}$$

Here N_I denotes the number of pixels in the reference (or test) image.

In order to make the estimates of the von Kries coefficient robust to the saturated pixels, from the summation

Figure 6: BARNARD: accuracies (12) and (13) of our method by varying N.

Illuminant	$\alpha_0 \pm \Delta\alpha_0$	$\alpha_1 \pm \Delta\alpha_1$	$\alpha_2 \pm \Delta\alpha_2$
syl-wwf	0.889 ± 0.176	0.657 ± 0.174	0.731 ± 0.162
syl-cwf	0.693 ± 0.198	0.808 ± 0.260	1.142 ± 0.368
syl-50MR16Q+3202	0.427 ± 0.127	0.616 ± 0.322	1.109 ± 0.348
solux-4700	0.474 ± 0.109	0.688 ± 0.163	1.054 ± 0.272
solux-4100	0.626 ± 0.116	0.821 ± 0.173	1.148 ± 0.261
solux-4100+3202	0.271 ± 0.088	0.496 ± 0.172	1.242 ± 0.486
solux-3500	0.936 ± 0.187	1.092 ± 0.223	1.219 ± 0.261
solux-3500+3202	0.379 ± 0.136	0.634 ± 0.239	1.281 ± 0.539
ph-ulm	0.869 ± 0.221	1.009 ± 0.292	0.806 ± 0.222
solux-4700+3202	0.218 ± 0.096	0.433 ± 0.200	1.200 ± 0.636

Table 1: Database BARNARD: estimated von Kries coefficients for $N = 256$ and $M = 100$.

in (16) we exclude the pairs $((\mathbf{p_i}^r)_j, (\mathbf{p_i}^t)_j)$ in which at least one element is 255.

Differently from BEST-FIT, the color transfer method presented in [4] is invariant to changes of size and in-plane orientation of the images. Like our method, color transfer employs statistical information about the color distribution of the images. Color transfer borrows the colors of an image onto an other. This approach is not tailored for the illuminant problem, but it is a general method largely used in Computer Graphics for correcting the color of an image with respect to a reference. The algorithm proposed in [4] (here denoted by CT) performs color transfer by means of a simple statistical analysis on the decorrelated orthogonal color space $l\alpha\beta$ [11]. Firstly the RGB responses of the reference image r and of the test image t are converted by a non-linear transform in the $l\alpha\beta$ space. For both the images, the mean values (indicated by the brackets $\langle \ \rangle$) and the standard deviations of the channels l, α, β are computed. The mean values are then subtracted from the sensor responses expressed in the $l\alpha\beta$ coordinates:

$$l^* = l - \langle l \rangle, \qquad \alpha^* = \alpha - \langle \alpha \rangle, \qquad \beta^* = \beta - \langle \beta \rangle$$

The color correction is performed by applying the transform

$$l' = \frac{\sigma_t^l}{\sigma_r^l} l^* + \langle l \rangle, \ \alpha' = \frac{\sigma_t^\alpha}{\sigma_r^\alpha} \alpha^* + \langle \alpha \rangle, \ \beta' = \frac{\sigma_t^\beta}{\sigma_r^\beta} \beta^* + \langle \beta \rangle$$

where σ_t and σ_r indicates the standard deviations of the coordinates in the superscript. The correction of the test image on the reference is then obtained by re-converting the new $l\alpha\beta$ coordinates into RGB. As for BEST-FIT, also for CT we remove from the computation of the mean and of the standard variations the pixels with value 255.

Table 2 shows the mean accuracies (averaged on the test sets) obtained on the datasets TESTS51, ALOI and BARNARD by our approach, BEST-FIT and CT and when no color enhancement is performed. The best results are obtained by BEST-FITS, but the discrepancy between the accuracies of BEST-FIT and our method is very small, while the worst results are given by CT. Moreover, thanks to the color description by normalized histograms, our approach (as well as CT) recovers the von Kries coefficients also in case of rescaled and/or rotated images, while BEST-FIT is not invariant to these transforms. In these experiments we set $N = 256$ and $M = 100$. The gap between the performances of CT and the other two methods is particularly remarkable for TESTS51, also when saturated pixels are removed from the mean and standard deviation computation. This is because the mean value used in CT captures just a small part of the color information.

Database	Mean Value of A_0	Mean Value of A in BEST-FIT	Mean Value of A in CT [4]	Mean Value of A in OUR APPROACH
TESTS51	0.7809	$3.7\ 10^{-7}$	0.9538	$7.0\ 10^{-6}$
ALOI	0.9913	0.9961	0.9959	0.9961
BARNARD	0.9447	0.9803	0.9772	0.9805

Table 2: Comparison of the mean accuracy obtained without applying any color balancing and by using BEST-FIT, the color transfer algorithm [4] and our approach.

4.5   Comparison with Color Constancy Algorithms

In this Section we compare our approach and BEST-FIT with the color constancy methods presented and tested in [31] on the dataset BARNARD.

The color constancy approaches considered in [31] are listed in Table 3. They include two Gray-World methods (GW and DB-GW), a version of the Retinex algorithm (SCALE-BY-MAX), several variants of a gamut mapping approach (CRULE-MV, CRULE-AVE, ECRULE-AVE, ECRULE-ICA, ECRULE-MV, CIP-AVE, CIP-MV, CIP-ICA), two neural network methods (SP-NEURAL-NET, NEURAL-NET), and some color by correlation techniques (C-by-C-MLM, C-by-C-MAP, C-by-C-MMSE, C-by-C-01). In AVE-ILLUM the illuminant of each image is assumed to be the average of the all illuminants in the database. NOTHING indicates that no color balancing has been applied. These algorithms have been applied on the dataset images to determine their illuminants. Several error measures are taken into account for computing the accuracy of the illuminant estimate. Here we consider two error measures, for which the results are available for all the color constancy methods in [31]. The first measure is the *angular error* between an illuminant $\mathcal{I}_{gt} = (p_0, p_1, p_2)$ of the ground-truth and its estimate $\mathcal{I}_e = (p_0^e, p_1^e, p_2^e)$:

$$E_0(\mathcal{I}_{gt}, \mathcal{I}_e) = \arccos \frac{\mathcal{I}_{gt} \cdot \mathcal{I}_e}{\parallel \mathcal{I}_{gt} \parallel \parallel \mathcal{I}_e \parallel}. \qquad (17)$$

Here $\parallel \cdot \parallel$ indicates the Euclidean norm.

The second measure is the L^2 distance between the chromaticities (r_{gt}, g_{gt}) and (r_e, g_e) of the illuminants $\mathcal{I}_{gt}$ and $\mathcal{I}_e$ respectively. The chromaticity of an illuminant (p_0, p_1, p_2) is the pair $(r = p_0/(p_0 + p_1 + p_2),\ g = p_1/(p_0 + p_1 + p_2))$. The chromaticity-based error on the illuminant estimate is defined as

$$E_1(\mathcal{I}_{gt}, \mathcal{I}_e) = \sqrt{(r_{gt} - r_e)^2 + (g_{gt} - g_e)^2}. \qquad (18)$$

Table 3 reports for each color constancy approach and for each $i = 0, 1$, the root mean square error computed as

$$\left[\frac{1}{Q} \sum_{(\mathcal{I}_{gt}, \mathcal{I}_e)} E_i(\mathcal{I}_{gt}, \mathcal{I}_e)^2 \right]^{\frac{1}{2}} \tag{19}$$

where Q is the total number of illuminant pairs $(\mathcal{I}_{gt}, \mathcal{I}_e)$ taken into account.

In BEST-FIT and in our approach, the illuminant of an image has been computed by scaling the canonical illuminant by the estimated von Kries coefficients. In our approach we used the finest color quantization ($N = 256$ bins, $M = 100$ bins).

There is a remarkable discrepancy between the errors output by BEST-FIT and by our approach and those obtained by the color constancy algorithms in [31]. This is due to the different inputs of the considered algorithms. In fact, the color constancy methods in [31] take as input just the canonical illuminant Ill_c and an image, and use them to estimate the illuminant of the image Ill_I. Then they compute the von Kries transform relating the Ill_c and the estimate of Ill_I and correct the input image as it would be captured under the reference illuminant.

BEST-FIT and our approach require as input a reference image (NOT the canonical illuminant) and a test image, and calculate the von Kries transform relating the reference to the test. Then they correct the test image by rescaling its channels according to the estimated von Kries coefficients. If Ill_c is known, the illuminant of the test image is estimated simply by scaling each components of Ill_c by the correspondent von Kries coefficient. Using a reference image instead of the canonical illuminant makes the estimate of the von Kries coefficients more accurate and therefore provides a better image correction.

While the color constancy approaches in [31] are successfully applied in Computer Graphics, for instance to improve the quality of digital photos, they are often not adequate for image and object recognition [30]. On the contrary, in Section 5 we prove that the color enhancement based on our estimate of the illuminant variation allows good performances in the illuminant invariant image recognition.

Algorithm	E_0 [degree]	E_1
NOTHING	17.9	0.125
AVE-ILLUM	12.9	0.094
GW	13.8	0.072
DB-GW	11.7	0.053
SCALE-BY-MAX	8.9	0.053
CIP-MV	23.4	0.149
CIP-AVE	16.1	0.105
CIP-ICA	10.6	0.076
NEURAL-NET	9.5	0.060
SP-NEURAL-NET	9.1	0.061

Algorithm	E_0 [degree]	E_1
C-by-C-01	10.9	0.072
C-by-C-MAP	9.9	0.063
C-by-C-MLM	9.9	0.062
C-by-C-MMSE	9.9	0.061
CRULE-MV	5.6	0.043
CRULE-AVE	7.1	0.046
ECRULE-MV	5.6	0.040
ECRULE-AVE	6.9	0.046
ECRULE-ICA	7.0	0.047
BEST-FIT	**1.9**	**0.015**
OUR-METHOD	**2.1**	**0.019**

Table 3: Database BARNARD: Comparison of the errors of our approach, BEST-FIT and of the color constancy algorithms presented in [31]. The errors of the methods in [31] have been reported in this Table as well as they are in [31] (see Table II first column, and Table III first column of [31]). An implementation of these approaches is available at `http://kobus.ca/research/code/colour_constancy/`.

5   Image Recognition

In this Section we show how the estimate of the von Kries transform can be used for achieving the illuminant invariant image recognition.

We stated the recognition problem as follows: let D be a database of known images (*references*), and let $\mathcal{F}$ a set of illuminant transformations, and let d be a dissimilarity measure between images. Given a new unknown image I (*query*), the recognition of I from D consists in finding the image I_0 of D and a transform T in $\mathcal{F}$ such that $d(T(I_0), I) = \min_{F \in \mathcal{F}, I_r \in D} d(F(I_r), I)$.

To find the reference (possibly relighted) most similar to an input query, we compute the von Kries transforms mapping each reference onto the query, and we associate a dissimilarity score to each of these transforms. The solution is the reference whose von Kries transform has the minimum dissimilarity from the query. In particular, we define the image dissimilarity as

$$\nabla = \sum_{i=0}^{2} \sum_{x=1}^{M} |\alpha_i \Psi_i(x) - \Psi_i'(x)|. \tag{20}$$

where Ψ_i and Ψ_i' are the inversions of the cumulative histograms of the ith channel of the query and reference respectively. We note the i-th term in (20) is the L^1 distance between the functions $\alpha_i \Psi_i$ and Ψ_i' ($i = 0, 1, 2$).

The dissimilarity score ∇ between a query I_r and a reference I depends on the transform K mapping I_r onto I, and therefore it is not a distance in the mathematical sense. In fact, because of it dependency on the von Kries coefficients, it does not satisfy triangular inequality. Nevertheless, ∇ is a *query-sensitive* dissimilarity measure, in the sense that it depends on the query. A mathematical formulation of the classification and retrieval problem in case of query-sensitive measures is illustrated in [2].

In the following, we say that a query I_r is *correctly* recognized if the reference image I of D minimizing (20) is a re-lighted version of I_r. The performance of our approach has been evaluated by the *recognition rate*, defined as the ratio between the number of test images correctly recognized and the total number of test images.

In our experiments, we considered the reference and the test sets of TESTS51 and ALOI defined in Section 3. When no color normalization is applied, the mean recognition rate is about 0.10 for TESTS51, and about 0.76 for ALOI.

Figure 7 shows the recognition rates of TESTS51 for different values of N, while Figure 8 shows the recognition rates for the different reference and test sets of ALOI when $N = 256$ (Right) and when no color enhancement is used (Left). An analysis about the recognition robustness with respect to the color quantization for the dataset ALOI is reported in Figure 9(Left), that shows for each reference set the mean recognition rate on all the test sets considered.

In the case of ALOI datasets, we compared our recognition rates with those obtained by using the color normalization methods Gray-World and ACE. We normalized the reference and query colors by Gray-World and ACE and we matched the color enhanced images by the dissimilarity measure (20) with $\alpha_i = 1.0$ for each $i = 0, 1, 2$. Figure 9(Right) shows, for each reference set, our recognition rates averaged on all the test sets, along with the recognition rates obtained by Gray World, ACE and without color enhancement. Both in terms of recognition rate and program run time, our approach and the Gray-World based method show similar results, while the use of ACE gives the worst performances. The smallest recognition rates output by our retrieval method are obtained for the lamp voltages V_{140} and V_{230}, that produce a large number of saturated pixels, determining a low accuracy on the determination of the von Kries coefficients and as consequence a decrement of the recognition performances. In fact, for these voltages the image brightness is higher than in the other cases.

6 Conclusions and Future Directions

In this paper we presented a new algorithm for computing the illuminant change possibly occurring between two images of a scene. Our approach approximates the illuminant variations with the von Kries model and hence assumes that the surfaces of the objects in the scene obey the Lambert's reflectance laws. The illuminant change between two pictures is computed by minimizing a dissimilarity measure between the piecewise inversions of
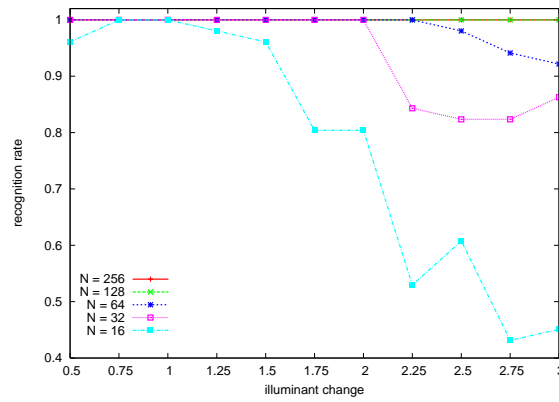
Figure 7: TESTS51: Robustness of the recognition rate with respect to different color histogram quantizations.
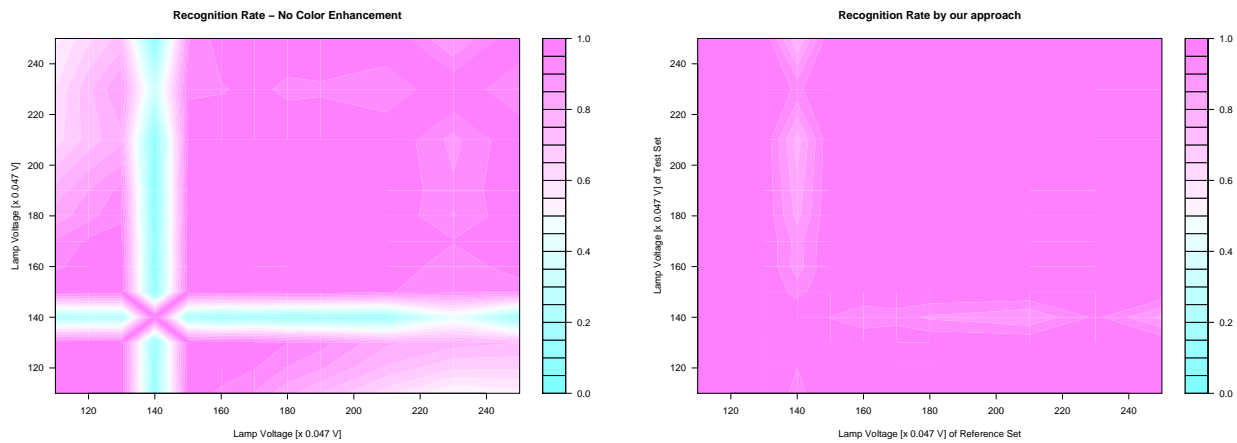

Figure 8: ALOI: Recognition rate for the different test and reference set when (Left) no color enhancement is applied; and (Right) by using our approach ($N = 256$, $M = 100$).
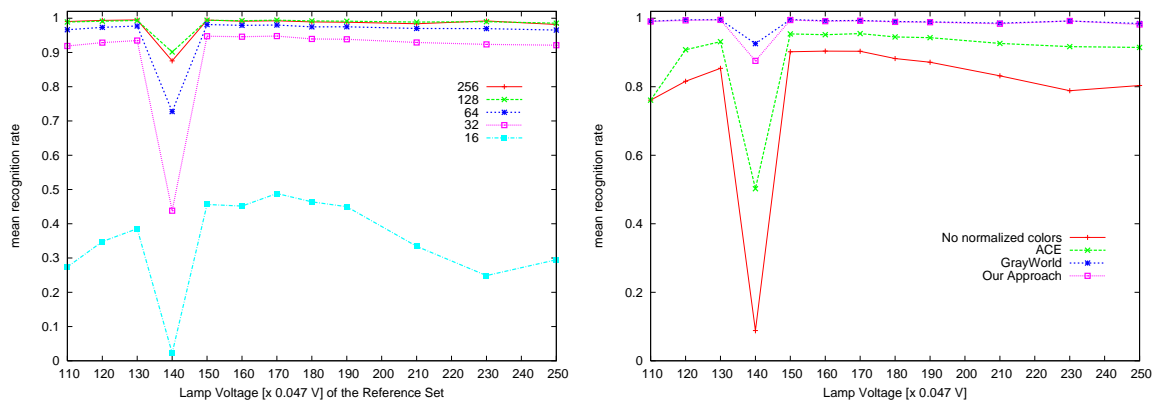

Figure 9: ALOI: (Left) Mean Recognition Rate averaged on the images of all the test sets versus color quantization and (Right) in comparison with Gray World and ACE, and without color balancing.

the cumulative color histograms of the considered images.

The main advantages of our estimate are: *i)* linear complexity with respect to the number of image pixels and to the color quantization, and consequent small run time for computing the von Kries coefficients (less than 0.04 seconds on an image of size 150×200 pixels on a standard CPU Pentium4, 2.8 GHz), *ii)* only two parameters to be set up (N and M), *iii)* robustness to pixel saturation, image rescaling and in-plane rotating.

The experiments illustrated in Section 4 showed a high accuracy on the computation of the von Kries transform and on the image color correction also by varying the color quantization parameters N and M. We compared our approach with a best-fit method and with the color constancy algorithms described in [31]. Differently from these color constancy techniques, given a single input image, our approach and BEST-FIT are not able to determine its illuminant. These simply compute the von Kries map relating two pictures, and provided the illuminant of one picture is known, they estimate that of the other. Nevertheless, BEST-FIT and our approach are more adequate for the illuminant invariant image recognition than the color constancy algorithms. Given a set of reference images and an unknown input image, the problem is to find the reference possibly relighted that is the most similar to the query. In this work we show how this goal can be achieved simply by estimating the von Kries coefficients relating the query to each reference and by using as dissimilarity measure the score (20). The proposed recognition method avoids the color correction step, necessary in the recognition approaches based on the color constancy methods, and guarantees higher performances. Moreover, differently from BEST-FIT, our method allows the recognition of rescaled and/or rotated images.

The retrieval results reported in Section 5 aim at showing how our algorithm compares to others when only color information is used, but we are aware that a color analysis cannot be sufficient for image recognition in the majority of the real world applications. In general other features, like texture and edges, are to be employed in addition to colors. In this framework, our technique can be integrated in a more complete object and image recognition system to provide information about possible changes of light and to enhance the image colors. In particular, we plan to integrate our technique in the object and image recognizer MEMORI [33], in order to make it invariant to changes of light. Moreover, we would like to investigate possible extensions of our approach to non Lambertian surfaces and to the case of non uniform illumination. Considered that the von Kries model cannot be applied on images taken with different devices, we are interested to develop new strategies or models in order to make our estimate *device-invariant*.

References

[1] V. Agarwal, A. V. Gribok, and M. A. Abidi. Neural networks letter: Machine learning approach to color constancy. In *Neural Netw.*, 20(5):559–563, 2007.

[2] V. Athitsos, M. Hadjieleftheriou, G. Kollios, and S. Sclaroff. Query-sensitive embeddings. In *SIGMOD '05: Proceedings of the 2005 ACM SIGMOD international conference on Management of data*, pgg. 706–717, New York, NY, USA, 2005. ACM Press.

[3] D. A. Forsyth, A novel algorithm for color constancy. In *Color*, 1992, pgg. 241–271

[4] E. Reinhard, M. Ashikhmin, B. Gooch, and P. Shirley. Color transfer between images. In *IEEE Comput. Graph. Appl.*, 21(5):34–41, 2001.

[5] G. D. Finlayson and S. D. Hordley and P. M. Hubel. Color by Correlation: A Simple, Unifying Framework for Color Constancy. In *IEEE Trans. Pattern Anal. Mach. Intell.* Vol. 23, N. 11, 2001, pgg. 1209–1221

[6] B. Funt, V. Cardei, K. Barnard Method of estimating chromaticity of illumination using neural networks. United States Patent 5907629, 1999

[7] J. Berens and G. Finlayson. Log-opponent chromaticity coding of colour space. In *15th IEEE Int. Conf. on Pattern Recognition*, pages 206–211, 2000.

[8] A. Rizzi, C. Gatta and D. Marini. ACE: An automatic color equalization algorithm. In *Proc. of CGIV2002 IS T*, Poitiers, France, 2002.

[9] V. C. Cardei, B. Funt, and K. Barnard. Estimating the scene illumination chromaticity by using a neural network. In *Journal of the Optical Society of America A*, 19:2374–2386, 2002.

[10] K. Deguchi, O. Kawanaka, and T. Okatani. Object tracking by the mean-shift of regional color distribution combined with the particle-filter algorithm. In *Proceedings of ICPR '04*, Vol. 3, pages 506–509, Washington, DC, USA, 2004. IEEE Computer Society.

[11] , D. L. Ruderman, Th. W. Cronin and C.C. Chiao, Statistics of Cone Responses to Natural Images: Implications for Visual Coding. In *J. of the Optical Society of America A*, Vol. 15, pages 2036–2045, 1998.

[12] , S. K. Nayar, E. Ikeuchi and T. Kanade, Surface reflection: Physical and geometrical perspectives. In *IEEE Transactions on Pattern Analysis and Machine Intelligence*, Vol. 13, pp. 611–634, 1991.

[13] L. T. Maloney, B. A. Wandell. Color Constancy: A Method for Recovering Surface Spectral Reflectance. In *J. Opt. Soc. Am. A*, Vol. 3, No. 1/Jan. 1986, pp. 29-33.

[14] A. Rizzi, E. Provenzi, L. De Carli. Mathematical definition and analysis of the Retinex algorithm. *Journal of the Optical Society of America.Optics, image science, and vision*, 22(12), 2005.

[15] G. Finlayson, S. Hordley, G. Schaefer, and G.Y. Tian. Illuminant and device invariance using histogram equalisation. In *IS&T and SID's 11th Color Imaging Conference*, pages 205–211, 2003.

[16] G. D. Finlayson, B. Schiele, and J. L. Crowley. Comprehensive colour image normalization. In *ECCV '98: Proceedings of the 5th European Conference on Computer Vision-Volume I*, pages 475–490, London, UK, 1998. Springer-Verlag.

[17] B. V. Funt and G. D. Finlayson. Color constant color indexing. In *IEEE Trans. Pattern Anal. Mach. Intell.*, 17(5):522–529, 1995.

[18] B. V. Funt, G. D. Finlayson, M. S. Drew. Diagonal transforms suffice for color constancy. In *Proc. of International Conference of Computer Vision*, 1993.

[19] J.M. Geusebroek, J. Loost van de Weijer, and T. Gevers. Edge and corner detection by photometric quasi-invariants. In *IEEE Trans. Pattern Anal. Mach. Intell.*, 27(4):625–630, 2005.

[20] J.M. Geusebroek, R. van den Boomgaard, A. W. M. Smeulders, and T. Gevers. Color constancy from physical principles. In *Pattern Recogn. Lett.*, 24(11):1653–1662, 2003.

[21] G. J. Burghouts, J. M. Geusebroek and A. W. M. Smeulders. The Amsterdam library of object images. *International Journal of Computer Vision*, 61(1):103–112, 2005.

[22] E. H. Land. The Retinex theory of color vision. In *Scientific American*, 237(6):108–128, 1977.

[23] D. G. Lowe. Distinctive image features from scale-invariant keypoints. *Int. J. Comput. Vision*, 60(2):91–110, 2004.

[24] D. Marimont and B. Wandell. Linear models of surface and illuminant spectra. In *J. Opt. Soc. Am.* A, Vol. 9, pp. 1905–1913, 1992.

[25] M. Ozden and E. Polat. A color image segmentation approach for content-based image retrieval. In *Pattern Recogn.*, 40(4):1318–1325, 2007.

[26] F. Rothganger, S. Lazebnik, C. Schmid, and J. Ponce. 3D object modeling and recognition using local affine-invariant image descriptors and multi-view spatial constraints. In *International Journal of Computer Vision*, 66(3):231–259, 2006.

[27] R. Schettini, G. Ciocca, and S. Zuffi. A survey of methods for colour image indexing and retrieval in image databases. In *Color Imaging Science: Exploiting Digital Media*, 2001.

[28] K. Barnard, L. Martin, B. Funt, and A. Coath. A data set for color research. In *Color Research and Application*, 27(3):148–152, 2002.

[29] K. Barnard, L. Martin, A. Coath, and B. Funt. A Comparison of Computational Color Constancy Algorithms; Part One: Theory and Experiments with Synthetic Data. In *IEEE Transactions in Image Processing*, 11(9):985–996, 2002.

[30] B. Funt, K. Barnard, L. Martin. Is Machine Color Constancy Enough? In *Proc. of ECCV 98*, 445–459, 1998 2002.

[31] K. Barnard, V. Cardei, and B. Funt. A comparison of computational color constancy algorithms. Part Two: Experiments with image data. In *Image Processing, IEEE Transactions on*, 11(9):985–996, 2002.

[32] M. Lecca, S. Messelodi. Estimating Illuminant Changes by Piecewise Inversion of Cumulative Color Histograms. *Technical Report*, FBK-irst Protocol Number 200806010.

[33] M. Lecca. Object recognition in color images by the self configuring system MEMORI. In *International Journal of Signal Processing* **3** (2006) 176–185

(a) $\alpha_0 \pm \Delta\alpha_0$

Voltage of the References	Voltage of the Tests											
	110	120	130	140	150	160	170	180	190	210	230	250
110	*	0.973 ± 0.020	1.116 ± 0.047	0.936 ± 0.030	0.902 ± 0.038	0.897 ± 0.040	0.871 ± 0.045	0.862 ± 0.047	0.834 ± 0.051	0.890 ± 0.045	0.820 ± 0.055	0.820 ± 0.055
120	1.011 ± 0.013	*	1.129 ± 0.049	0.947 ± 0.025	0.912 ± 0.033	0.907 ± 0.035	0.881 ± 0.040	0.872 ± 0.042	0.843 ± 0.047	0.900 ± 0.041	0.829 ± 0.050	0.829 ± 0.050
130	1.028 ± 0.021	1.016 ± 0.013	*	0.962 ± 0.019	0.927 ± 0.028	0.922 ± 0.030	0.896 ± 0.036	0.886 ± 0.038	0.857 ± 0.044	0.915 ± 0.036	0.843 ± 0.047	0.843 ± 0.047
140	0.898 ± 0.037	0.887 ± 0.038	0.873 ± 0.040	*	0.807 ± 0.053	0.803 ± 0.054	0.779 ± 0.058	0.770 ± 0.059	0.744 ± 0.062	0.796 ± 0.057	0.731 ± 0.063	0.731 ± 0.063
150	1.070 ± 0.035	1.057 ± 0.028	1.040 ± 0.021	1.197 ± 0.067	*	0.959 ± 0.019	0.931 ± 0.026	0.921 ± 0.029	0.891 ± 0.034	0.951 ± 0.026	0.877 ± 0.038	0.877 ± 0.038
160	1.111 ± 0.047	1.098 ± 0.040	1.079 ± 0.033	1.244 ± 0.082	1.038 ± 0.016	*	0.966 ± 0.018	0.956 ± 0.021	0.925 ± 0.027	0.987 ± 0.021	0.910 ± 0.031	0.910 ± 0.031
170	1.117 ± 0.050	1.104 ± 0.043	1.086 ± 0.036	1.252 ± 0.085	1.044 ± 0.021	1.006 ± 0.011	*	0.961 ± 0.018	0.930 ± 0.024	0.992 ± 0.020	0.915 ± 0.029	0.915 ± 0.029
180	1.151 ± 0.060	1.137 ± 0.053	1.118 ± 0.046	1.291 ± 0.097	1.075 ± 0.030	1.035 ± 0.019	1.030 ± 0.014	*	0.957 ± 0.018	1.021 ± 0.019	0.942 ± 0.024	0.942 ± 0.024
190	1.164 ± 0.064	1.150 ± 0.057	1.131 ± 0.049	1.306 ± 0.101	1.086 ± 0.034	1.047 ± 0.023	1.041 ± 0.019	1.011 ± 0.011	*	1.032 ± 0.019	0.952 ± 0.021	0.952 ± 0.021
210	1.204 ± 0.075	1.190 ± 0.068	1.170 ± 0.060	1.353 ± 0.113	1.124 ± 0.044	1.082 ± 0.032	1.076 ± 0.029	1.045 ± 0.020	1.034 ± 0.014	*	0.984 ± 0.016	0.984 ± 0.016
230	1.127 ± 0.059	1.114 ± 0.051	1.095 ± 0.044	1.263 ± 0.092	1.052 ± 0.030	1.014 ± 0.022	1.009 ± 0.020	0.980 ± 0.018	0.969 ± 0.017	0.938 ± 0.019	*	0.922 ± 0.021
250	1.225 ± 0.083	1.210 ± 0.075	1.190 ± 0.067	1.378 ± 0.119	1.143 ± 0.050	1.100 ± 0.038	1.094 ± 0.035	1.063 ± 0.027	1.051 ± 0.024	1.017 ± 0.016	1.085 ± 0.024	*

(b) $\alpha_1 \pm \Delta\alpha_1$

Voltage of the References	Voltage of the Tests											
	110	120	130	140	150	160	170	180	190	210	230	250
110	*	1.025 ± 0.026	1.238 ± 0.071	1.025 ± 0.034	1.002 ± 0.036	1.014 ± 0.038	0.999 ± 0.040	1.003 ± 0.041	0.995 ± 0.043	1.076 ± 0.052	0.989 ± 0.047	0.989 ± 0.047
120	0.982 ± 0.017	*	1.216 ± 0.062	1.006 ± 0.027	0.984 ± 0.029	0.996 ± 0.032	0.981 ± 0.034	0.985 ± 0.035	0.977 ± 0.037	1.057 ± 0.044	0.972 ± 0.040	0.972 ± 0.040
130	0.976 ± 0.024	0.993 ± 0.016	*	0.999 ± 0.020	0.978 ± 0.024	0.989 ± 0.026	0.974 ± 0.029	0.978 ± 0.030	0.971 ± 0.032	1.050 ± 0.038	0.965 ± 0.035	0.965 ± 0.035
140	0.810 ± 0.046	0.825 ± 0.043	0.830 ± 0.040	*	0.812 ± 0.043	0.821 ± 0.043	0.809 ± 0.046	0.812 ± 0.046	0.806 ± 0.047	0.871 ± 0.040	0.801 ± 0.049	0.801 ± 0.049
150	0.977 ± 0.032	0.994 ± 0.026	1.001 ± 0.020	1.208 ± 0.056	*	0.990 ± 0.019	0.975 ± 0.023	0.979 ± 0.024	0.971 ± 0.026	1.050 ± 0.031	0.965 ± 0.029	0.965 ± 0.029
160	0.999 ± 0.036	1.017 ± 0.030	1.024 ± 0.025	1.236 ± 0.065	1.023 ± 0.014	*	0.997 ± 0.019	1.001 ± 0.021	0.993 ± 0.023	1.074 ± 0.032	0.987 ± 0.027	0.987 ± 0.027
170	0.987 ± 0.037	1.005 ± 0.032	1.012 ± 0.027	1.221 ± 0.063	1.011 ± 0.020	0.988 ± 0.013	*	0.989 ± 0.018	0.981 ± 0.021	1.061 ± 0.029	0.976 ± 0.025	0.976 ± 0.025
180	1.003 ± 0.040	1.020 ± 0.035	1.027 ± 0.031	1.240 ± 0.069	1.026 ± 0.024	1.004 ± 0.019	1.015 ± 0.014	*	0.996 ± 0.018	1.077 ± 0.030	0.990 ± 0.023	0.990 ± 0.023
190	0.999 ± 0.041	1.017 ± 0.036	1.023 ± 0.032	1.235 ± 0.069	1.023 ± 0.025	1.000 ± 0.021	1.012 ± 0.018	0.996 ± 0.012	*	1.073 ± 0.027	0.987 ± 0.022	0.987 ± 0.022
210	1.007 ± 0.043	1.025 ± 0.038	1.031 ± 0.034	1.245 ± 0.072	1.031 ± 0.028	1.020 ± 0.024	1.020 ± 0.022	1.004 ± 0.019	1.008 ± 0.013	*	0.994 ± 0.018	0.994 ± 0.018
230	0.931 ± 0.045	0.948 ± 0.039	0.954 ± 0.034	1.150 ± 0.053	0.953 ± 0.028	0.932 ± 0.028	0.943 ± 0.025	0.929 ± 0.025	0.932 ± 0.023	0.925 ± 0.020	*	0.920 ± 0.020
250	1.013 ± 0.049	1.031 ± 0.043	1.038 ± 0.039	1.253 ± 0.076	1.037 ± 0.032	1.014 ± 0.028	1.026 ± 0.026	1.010 ± 0.024	1.014 ± 0.023	1.006 ± 0.018	1.088 ± 0.023	*

(c) $\alpha_2 \pm \Delta\alpha_2$

Voltage of the References	Voltage of the Tests											
	110	120	130	140	150	160	170	180	190	210	230	250
110	*	1.082 ± 0.047	1.408 ± 0.088	1.131 ± 0.073	1.123 ± 0.081	1.162 ± 0.091	1.163 ± 0.097	1.189 ± 0.105	1.217 ± 0.116	1.355 ± 0.137	1.226 ± 0.123	1.226 ± 0.123
120	0.954 ± 0.027	*	1.342 ± 0.065	1.077 ± 0.050	1.070 ± 0.059	1.107 ± 0.068	1.107 ± 0.074	1.132 ± 0.080	1.159 ± 0.091	1.291 ± 0.109	1.167 ± 0.097	1.167 ± 0.097
130	0.926 ± 0.040	0.970 ± 0.023	*	1.044 ± 0.035	1.037 ± 0.044	1.073 ± 0.053	1.073 ± 0.059	1.097 ± 0.065	1.122 ± 0.075	1.250 ± 0.091	1.130 ± 0.081	1.130 ± 0.081
140	0.713 ± 0.045	0.747 ± 0.037	0.770 ± 0.031	*	0.798 ± 0.038	0.826 ± 0.042	0.826 ± 0.046	0.844 ± 0.049	0.864 ± 0.054	0.961 ± 0.057	0.870 ± 0.058	0.870 ± 0.058
150	0.888 ± 0.058	0.930 ± 0.043	0.959 ± 0.032	1.246 ± 0.048	*	1.027 ± 0.031	1.027 ± 0.037	1.050 ± 0.043	1.075 ± 0.051	1.196 ± 0.064	1.082 ± 0.057	1.082 ± 0.057
160	0.895 ± 0.066	0.937 ± 0.052	0.966 ± 0.041	1.255 ± 0.058	1.007 ± 0.020	*	1.034 ± 0.029	1.057 ± 0.035	1.082 ± 0.044	1.204 ± 0.058	1.089 ± 0.049	1.089 ± 0.049
170	0.866 ± 0.070	0.907 ± 0.057	0.935 ± 0.046	1.214 ± 0.060	0.974 ± 0.029	0.967 ± 0.018	*	1.022 ± 0.027	1.046 ± 0.035	1.164 ± 0.049	1.053 ± 0.041	1.053 ± 0.041
180	0.866 ± 0.075	0.907 ± 0.062	0.935 ± 0.052	1.215 ± 0.067	0.975 ± 0.036	0.968 ± 0.027	1.000 ± 0.019	*	1.046 ± 0.030	1.164 ± 0.045	1.053 ± 0.038	1.053 ± 0.038
190	0.848 ± 0.078	0.888 ± 0.065	0.915 ± 0.056	1.188 ± 0.069	0.954 ± 0.039	0.947 ± 0.032	0.979 ± 0.026	0.979 ± 0.017	*	1.139 ± 0.038	1.030 ± 0.032	1.030 ± 0.032
210	0.830 ± 0.083	0.868 ± 0.071	0.895 ± 0.061	1.162 ± 0.074	0.933 ± 0.045	0.926 ± 0.037	0.957 ± 0.033	0.957 ± 0.027	0.978 ± 0.019	*	1.007 ± 0.025	1.007 ± 0.025
230	0.746 ± 0.078	0.781 ± 0.068	0.804 ± 0.060	1.044 ± 0.064	0.838 ± 0.045	0.832 ± 0.040	0.860 ± 0.036	0.860 ± 0.033	0.879 ± 0.029	0.899 ± 0.022	*	0.905 ± 0.019
250	0.825 ± 0.087	0.863 ± 0.075	0.889 ± 0.066	1.155 ± 0.079	0.927 ± 0.049	0.920 ± 0.042	0.951 ± 0.038	0.951 ± 0.034	0.972 ± 0.030	0.994 ± 0.024	1.106 ± 0.023	*

Table 4: ALOI: Estimates of α_0, α_1, α_2 with error and $N = 256$. The entry kj of each Table is the mean value of the coefficients of the von Kries map between the test images illuminated with voltage V_k and the reference taken with voltage V_j, and $\Delta\alpha_i$ is the standard deviation of the von Kries coefficient estimates.